

Nonlinear vibration transfer in torsion pendulums

Tomofumi Shimoda & Masaki Ando

Department of physics, University of Tokyo, 7-3-1, Hongo, Bunkyo-ku, Tokyo
113-0033, Japan

E-mail: shimoda@granite.phys.s.u-tokyo.ac.jp

December 2018

Abstract. Torsion pendulums have been widely used in physical experiments, because their small restoring forces are suitable for tiny force measurement. Recently, some applications such as low-frequency gravity gradiometers have been proposed by focusing on their low resonant frequencies. Torsion pendulums with low resonant frequencies enable the suspended masses to be isolated from the ground, allowing for good response to the fluctuation of local gravity field at low frequencies. However, translational ground vibration can be transferred to the horizontal rotation of the torsion pendulum nonlinearly. This effect can have a non-negligible contribution to the sensitivity of torsion pendulums as gravity gradiometers. This paper evaluates the amount of nonlinear vibration noise, and discusses how to reduce it.

Keywords: Torsion pendulum, Gravitational wave, Earthquake early warning

1. Introduction

A torsion pendulum is a long-standing tool in physical experiments. Its small restoring force enables tiny force measurements such as those required in gravitational experiments. Hence it has been used for the test of gravitational inverse-square law [1, 2], measurement of Newton's gravitational constant G (e.g. [3, 4, 5]) and other experiments.

Recently, Torsion-Bar Antenna (TOBA), a local gravity gradiometer using a torsion pendulum, has also been proposed and is being developed [6, 7, 8]. It utilizes the low resonant frequency of a torsion pendulum (\sim a few mHz), which leads the pendulum to behave like a free-falling body down to the resonant frequency. This enables a good response to gravitational waves (GWs) and passive isolation of rotational vibration of the suspension point above the resonant frequency. Hence a torsion pendulum can have good sensitivity to GWs at low frequencies even on land. This configuration is also expected to be useful for earthquake early warning (EEW) by measuring gravity perturbations [9, 10, 11]. The similar detector TorPeDO (Torsion Pendulum Dual Oscillator) is currently under development for the purpose of such terrestrial gravity

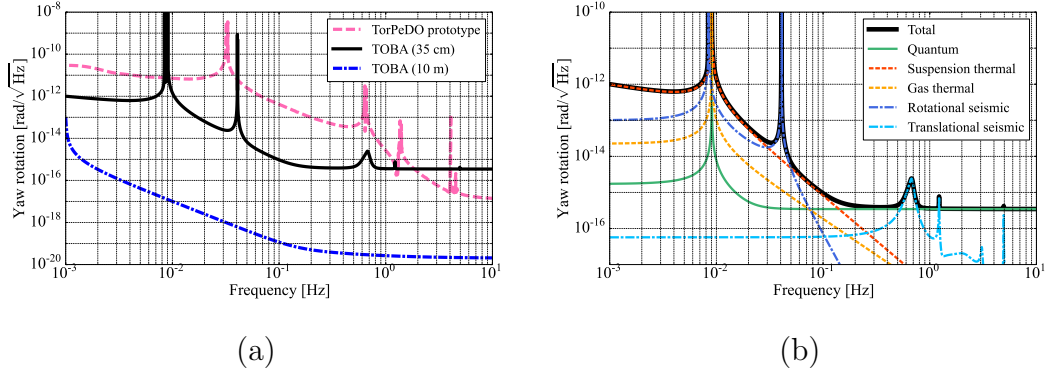


Figure 1. (a) The target sensitivities of proposed gravity gradiometers and/or their prototypes : prototype of TorPeDO (dashed pink), TOBA with 35 cm bars (solid black), and TOBA with 10 m bars (dot-dashed blue). (b) The noise budget of TOBA with 35 cm bars. It is mainly limited by quantum noise (solid green) and thermal noise of the suspension wires (dashed red), and partly limited by rotational (dot-dashed blue) and translational (dot-dashed light blue) seismic noise, which are linearly transferred to the horizontal rotation of the bars. Thermal noise of residual gas (dashed orange) is not dominant.

measurements [12, 13]. Fig. 1 shows the target sensitivities of these detectors and/or their prototypes [6, 12]. The target noise level is roughly about 10^{-15} rad/√Hz around 0.1 Hz for EEW, and 10^{-19} rad/√Hz for GWs. In the Fig. 1 (b), the main noise sources of TOBA with 35 cm bars are plotted for comparison against the nonlinear vibration noise discussed in this paper.

In these applications, seismic noise is one of the noise sources which can limit sensitivity. The rotational motion of the ground can be easily isolated with a multi-stage torsion pendulum, which works as a passive vibration isolation system. The horizontal rotational of the pendulum induced by the translational motion of the ground, called “cross-coupling”, has also been investigated. It was found that the linear cross-coupling transfer is caused by the asymmetry of the system, so it can be suppressed by improving the symmetry [14]. However, even if the pendulum is completely symmetric in its stationary state, vibration of the ground induces momentary asymmetry of the pendulum, which creates nonlinear cross-coupling. This effect has not been studied so far in terms of noise of the pendulum.

In this paper, the nonlinear vibration transfer in a torsion pendulum is investigated. The principle of this transfer is explained in Sec. 2, which is evaluated for some cases, followed by a discussion on how to reduce it in Sec. 3 and 4.

2. Nonlinear vibration transfer

The purpose of this section is to derive the explicit formula of horizontal (Yaw) rotation induced by nonlinear vibration transfer, and see what parameters are important for it. The definition of the coordinates and parameters of the system are shown in Fig.

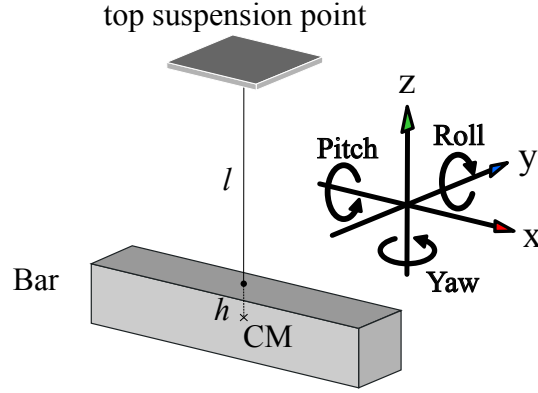


Figure 2. The model of a torsion pendulum and definition of coordinates.

2. The length of the suspension wire is defined as l , and the distance between the suspension point and the center of mass (CM) is h . In the following discussion, (x, y, z) is the position of the CM, and $(\theta_P, \theta_R, \theta_Y)$ is the rotational angle around the CM. The subscripts P, R and Y indicates Pitch, Roll and Yaw, respectively. The horizontal translations of the ground are expressed as x_g and y_g .

2.1. Derivation

The Lagrangian of the system is

$$\mathcal{L} = \frac{1}{2}m(\dot{x}^2 + \dot{y}^2) + \frac{1}{2}\vec{\omega} \cdot \mathbf{I}\vec{\omega} - mgz - \frac{1}{2}\kappa_Y\theta_Y^2 \quad (1)$$

and the dissipation function is defined as

$$\mathcal{D} = \frac{1}{2}\Gamma_x\dot{x}^2 + \frac{1}{2}\Gamma_y\dot{y}^2 + \frac{1}{2}\Gamma_P\dot{\theta}_P^2 + \frac{1}{2}\Gamma_R\dot{\theta}_R^2 + \frac{1}{2}\Gamma_Y\dot{\theta}_Y^2 \quad (2)$$

Here we take the kinetic energy, gravitational potential and elastic energy of the torsional mode of the wire into account. The elastic energy about the bending of the wire is ignored here by assuming that the wire is thin enough. m and \mathbf{I} are the mass and the moment tensor of the bar, $\vec{\omega} = \frac{d}{dt}(\theta_P, \theta_R, \theta_Y)$ is the angular velocity vector, and κ_Y is the torsional spring constant of the wire. Γ_α ($\alpha = x, y, P, R, Y$) is a damping coefficient of each degree of freedom. In the following discussion, the displacement is assumed to be small enough so that the small angle approximation ($\sin \theta \simeq \theta$ and $\cos \theta \simeq 1 - \theta^2/2$) is valid. In Eq. (1) and the following equations, (t) of the time-domain variables, such as $x, y, z, \theta_P, \theta_R$ or θ_Y , are omitted. Since the purpose of this calculation is the nonlinear effect, a time-varying moment tensor $\mathbf{I}(t)$ has to be used. Its non-diagonal elements are caused by the Pitch and the Roll rotations induced by the seismic vibration, and is

$$\mathbf{I}(t) = \begin{pmatrix} I_P & 0 & \theta_R(I_Y - I_P) \\ 0 & I_R & \theta_P(I_R - I_Y) \\ \theta_R(I_Y - I_P) & \theta_P(I_R - I_Y) & I_Y \end{pmatrix}. \quad (3)$$

Here I_P, I_R and I_Y are moments of inertia around principal axes of the suspended bar. The vertical position of the center of mass (CM), z , can be calculated geometrically. As

seismically excited vibrations of a typical pendulum considered here are almost always below 10^{-5} m/ $\sqrt{\text{Hz}}$ for translations and 10^{-4} rad/ $\sqrt{\text{Hz}}$ for vertical rotations, as shown later in Fig. 3 (b), the lowest order terms of x/h , y/h , θ_P and θ_R are larger than the higher order terms by at least two orders of magnitude in the following calculations. By ignoring the third and higher order terms, the time-domain expression of z is

$$z \simeq \frac{1}{2l} \left\{ (x + h\theta_R + h\theta_P\theta_Y - x_g)^2 + (y - h\theta_P + h\theta_R\theta_Y - y_g)^2 \right\} + \frac{1}{2}h(\theta_P^2 + \theta_R^2). \quad (4)$$

The non-diagonal elements of Eq. (3) and the cross terms between θ_Y and θ_P or θ_R in Eq. (4) are the source of nonlinear vibration transfer to Yaw rotation.

The Euler-Lagrange equations can be derived from (1) with (3) and (4). The equations for x and y are

$$m\ddot{x} = -\frac{mg}{l}(x + h\theta_R + h\theta_P\theta_Y - x_g) - \Gamma_x\dot{x} \quad (5)$$

and

$$m\ddot{y} = -\frac{mg}{l}(y - h\theta_P + h\theta_R\theta_Y - y_g) - \Gamma_y\dot{y}. \quad (6)$$

By using these equations, we get the equation for θ_Y as

$$\kappa_Y\theta_Y + I_Y\ddot{\theta}_Y = -(I_R - I_Y)\theta_P\ddot{\theta}_R - (I_Y - I_P)\ddot{\theta}_P\theta_R + (I_P - I_R)\dot{\theta}_P\dot{\theta}_R - mh(\ddot{x}\theta_P + \ddot{y}\theta_R). \quad (7)$$

Here the dissipation terms are assumed to be much smaller than the other terms, *e.g.* $m\ddot{x} \gg \Gamma_x\dot{x}$, and ignored for simplicity. In the frequency-domain, the Fourier-transformed Yaw angle $\tilde{\theta}_Y$ is

$$\tilde{\theta}_Y = \frac{1}{\kappa_Y - I_Y\omega^2} \left[(I_R - I_Y)\tilde{\theta}_P * (\omega^2\tilde{\theta}_R) + (I_Y - I_P)(\omega^2\tilde{\theta}_P) * \tilde{\theta}_R - (I_P - I_R)(\omega\tilde{\theta}_P) * (\omega\tilde{\theta}_R) + mh \left\{ (\omega^2\tilde{x}) * \tilde{\theta}_P + (\omega^2\tilde{y}) * \tilde{\theta}_R \right\} \right]. \quad (8)$$

Here “*” means frequency convolution defined by

$$(F * G)(f) = \int_{-\infty}^{\infty} F(x)G(f - x)dx \quad (F(f), G(f) : \text{functions}). \quad (9)$$

The noise spectrum of Yaw rotation, which is the main target of this paper, can be calculated from \tilde{x} , \tilde{y} , $\tilde{\theta}_P$ and $\tilde{\theta}_R$ by using Eq. (8). The terms inside the square brackets are the nonlinear torque noise. In calculating \tilde{x} , \tilde{y} , $\tilde{\theta}_P$ and $\tilde{\theta}_R$, the nonlinear effect does not have to be considered. As shown in Eq. (5) and (6), the nonlinear terms (the third term in the bracket of each equation) are smaller than the other terms by the order of θ_Y , which is at most 10^{-5} rad rms as calculated later (Fig. 4). Hence they are dominated by linearly induced motions. Under this condition, the equations of motion about x , y , θ_P and θ_R are

$$m\ddot{x} = -\frac{mg}{l}(x + h\theta_R - x_g) - \Gamma_x\dot{x}, \quad (10)$$

$$m\ddot{y} = -\frac{mg}{l}(y - h\theta_P - y_g) - \Gamma_y\dot{y}, \quad (11)$$

$$I_P\ddot{\theta}_P = \frac{mgh}{l}(y - h\theta_P - y_g) - mgh\theta_P - \Gamma_P\dot{\theta}_P, \quad (12)$$

$$I_R\ddot{\theta}_R = -\frac{mgh}{l}(x + h\theta_R - x_g) - mgh\theta_R - \Gamma_R\dot{\theta}_R. \quad (13)$$

Assuming $l \gg h$, \tilde{x} , \tilde{y} , $\tilde{\theta}_P$ and $\tilde{\theta}_R$ are approximated to

$$\tilde{x} \simeq \frac{f_x^2}{f_x^2 + i\frac{f_x}{Q_x}f - f^2} \tilde{x}_g, \quad (14)$$

$$\tilde{y} \simeq \frac{f_y^2}{f_y^2 + i\frac{f_y}{Q_y}f - f^2} \tilde{y}_g, \quad (15)$$

$$\tilde{\theta}_P \simeq \frac{4\pi^2 f_y^2 f_P^2 f^2}{g \left(f_y^2 + i\frac{f_y}{Q_y}f - f^2 \right) \left(f_P^2 + i\frac{f_P}{Q_P}f - f^2 \right)} \tilde{y}_g, \quad (16)$$

$$\tilde{\theta}_R \simeq -\frac{4\pi^2 f_x^2 f_R^2 f^2}{g \left(f_x^2 + i\frac{f_x}{Q_x}f - f^2 \right) \left(f_R^2 + i\frac{f_R}{Q_R}f - f^2 \right)} \tilde{x}_g. \quad (17)$$

Here the damping coefficients Γ_α ($\alpha = x, y, P, R$) have been converted into the Q factors Q_α . The resonant frequencies f_x , f_y , f_P and f_R are

$$f_x \simeq f_y \simeq \frac{1}{2\pi} \sqrt{\frac{g}{l+h}}, \quad f_P \simeq \frac{1}{2\pi} \sqrt{\frac{mgh}{I_P}}, \quad \text{and} \quad f_R \simeq \frac{1}{2\pi} \sqrt{\frac{mgh}{I_R}}. \quad (18)$$

As Eq. (8) shows, the nonlinear torque depends on the mass, the moments of inertia, the height of suspension point, as well as the amplitudes of x , y translations and Roll, Pitch rotations.

2.2. Calculation

The amount of vibration is calculated here. The model pendulum is a 30 cm \times 4 cm \times 3cm bar-shaped mass, whose parameters are listed in Table 1. Two seismic vibration spectrum models are assumed here, which are shown with the blue solid line and dashed line in Fig. 3 (a). Their respective Trans, Long, Roll and Pitch vibration spectrums along with their resonant modes are shown in Fig. 3 (b). The noisier environment model is close to the measured spectrum in Tokyo, while other less populated places have a similar level as the quiet model. Seismic vibration spectrums at several sites are summarized in [15]. The phase of the seismic vibration at each frequency is assumed to be random, *i.e.* the vibration at different frequencies are uncorrelated to each other.

The calculation results from Eq. (8) for the two seismic vibration models are shown in Fig. 4 with blue lines. The contribution from the first three terms of Eq. (8), which are related to the moments of inertia, is drawn with the pink line. The last term of Eq. (8), which is proportional to the mass, is shown with the orange line. They are dominant at higher and lower frequencies, respectively, and their cross-over frequency is 0.3 Hz in this case.

Total torsion angle noise is about 10^{-9} rad/ $\sqrt{\text{Hz}}$ for the seismically noisy case and 10^{-11} rad/ $\sqrt{\text{Hz}}$ for the quiet case at 0.1 Hz. In terms of torque, they correspond to 3×10^{-11} N \cdot m/ $\sqrt{\text{Hz}}$ and 3×10^{-13} N \cdot m/ $\sqrt{\text{Hz}}$, respectively. Since the nonlinear Yaw rotation originates from the convolution of two degrees of freedom, reduction of seismic vibration by one order of magnitude results in a two orders of magnitude suppression of nonlinear noise. In any case, nonlinear noise is much higher than the other noise sources

Table 1. The parameters used for the calculation.

parameter		symbol	value	unit
mass		m	1.0	kg
moment of inertia	(Pitch)	I_P	0.23×10^{-3}	$\text{kg}\cdot\text{m}^2$
	(Roll)	I_R	7.64×10^{-3}	$\text{kg}\cdot\text{m}^2$
	(Yaw)	I_Y	7.58×10^{-3}	$\text{kg}\cdot\text{m}^2$
length of wire		l	0.3	m
suspension point height		h	0.005	0.15 m
Q factors		Q_x, Q_y, Q_P, Q_R	10^3	-
resonant frequency	translation (x)	f_x	0.912	Hz
	translation (y)	f_y	0.901	Hz
	Pitch	f_P	2.469	Hz
	Roll	f_R	0.405	Hz

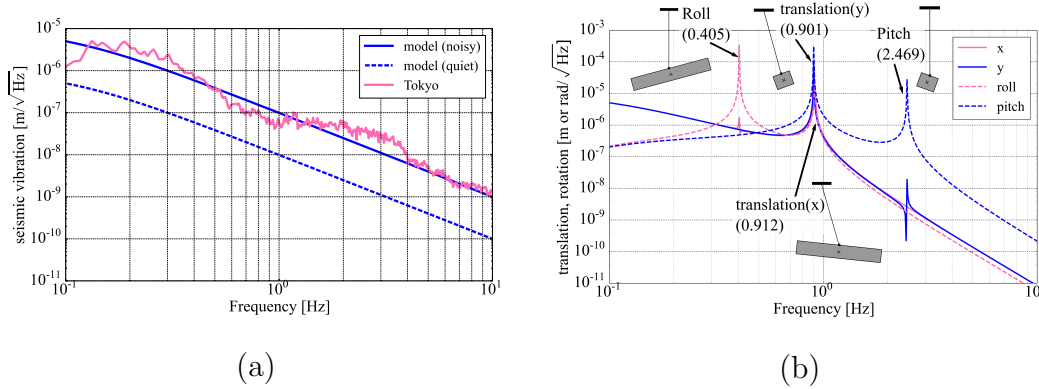


Figure 3. (a) The amplitude spectral density (ASD) of assumed seismic vibration models for a noisy case (blue solid line) and a quiet case (blue dashed line). Vibrations measured in Tokyo (pink) is also shown for comparison. (b) The respective pendulum's translations (x and y) and rotations (Roll and Pitch) for noisy model of seismic vibrations. Four resonant modes are drawn and their frequencies are indicated in the bracket.

and cannot be ignored at the target sensitivity as a gravity gradiometer, which is at least 10^{-15} rad/ $\sqrt{\text{Hz}}$ at 0.1 Hz. Therefore we need a strategy to suppress the nonlinear noise, which will be discussed in the next section.

The amplitude spectral density (ASD) in Fig. 4 has many peaks. The frequencies of these peaks correspond to the sum or the difference of the resonant frequencies of the translational modes in x , y , Roll and Pitch modes, since the Yaw rotation is induced by the frequency convolutions of these degrees of freedom. For example, the peak at 0.5 Hz originates from the 0.9 Hz resonance of the translational mode in y and the 0.4 Hz resonance of the Roll rotational mode, which are convolved via the last term of Eq. (8).

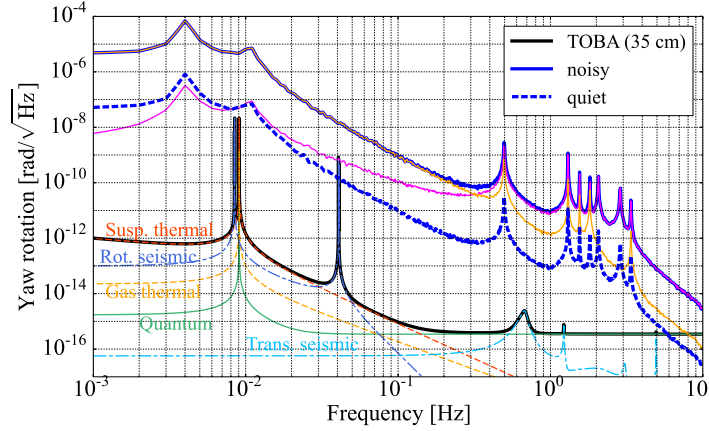


Figure 4. The calculated amplitude spectral density of nonlinearly induced Yaw rotation for large vibration case (solid blue line) and quiet case (dashed blue line). For the case of noisy ground vibration, the solid pink line is the sum of the first three terms of Eq. (8), and the solid orange line shows the last term of Eq. (8). The target sensitivity of TOBA with 35 cm bars is shown with the solid black line, with the noise sources shown in Fig. 1 (b).

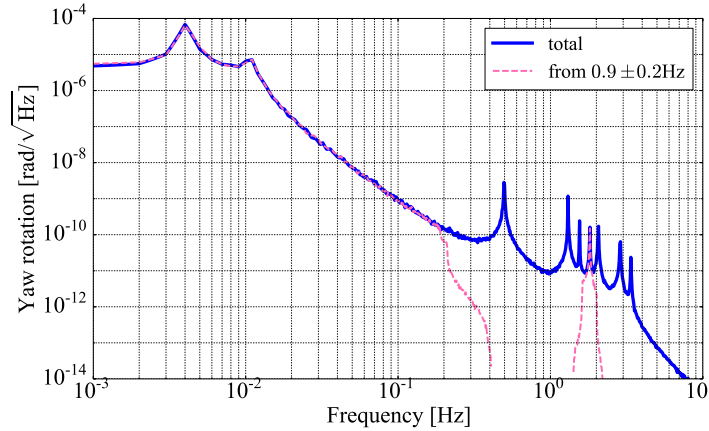


Figure 5. The calculated nonlinear noise (solid blue, same as Fig. 4) and the contribution from around the translational resonance peaks, with \tilde{x} , \tilde{y} , $\tilde{\theta}_P$ and $\tilde{\theta}_R$ limited to 0.9 ± 0.2 Hz (dashed pink).

3. Reduction of nonlinear vibration noise

In this section we discuss how to reduce the nonlinear vibration noise. The discussion is based on Eq. (8). To do so, we first give an analytic formula of the frequency convolution with some approximations.

The dashed pink line in Fig. 5 is the contribution from the frequency range around the translational resonance (0.9 Hz), which is calculated from Eq. (8) by limiting the

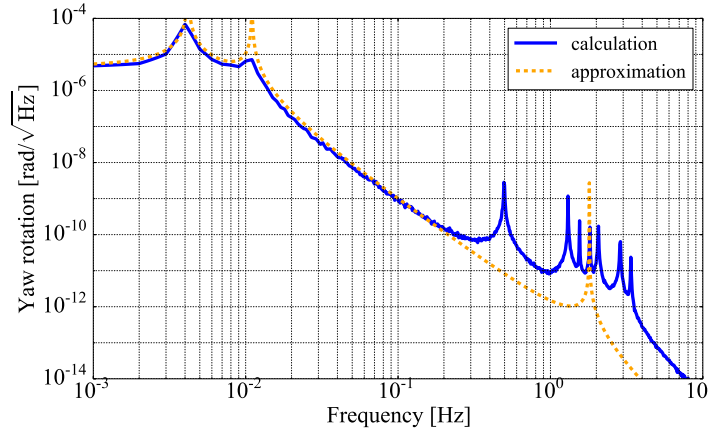


Figure 6. The approximated formula Eq. (19) (dotted orange) and the full calculation result (solid blue). The approximation is close to the full calculation below 0.3 Hz.

frequency range of \tilde{x} , \tilde{y} , $\tilde{\theta}_P$ and $\tilde{\theta}_R$ to 0.9 ± 0.2 Hz. It has a dominant contribution to the total ASD below 0.2 Hz. This is because the resonant frequencies of x or θ_R and of y or θ_P are very close (0.912 Hz and 0.901 Hz) so that the convolution between their peaks becomes large. Therefore, total nonlinear noise can be approximated by the convolution between these resonant peaks. Additionally, as shown in Fig. 4, the terms of $(\omega^2 \tilde{x}) * \tilde{\theta}_P$ and $(\omega^2 \tilde{y}) * \tilde{\theta}_R$ of Eq. (8) are dominant below 0.3 Hz. Since Pitch rotation is larger than Roll rotation around 0.9 Hz (Fig. 3 (b)), $(\omega^2 \tilde{x}) * \tilde{\theta}_P$ is the most important term for the approximation.

The amplitude spectral density of the convolution term $(\omega^2 \tilde{x}) * \tilde{\theta}_P$ is calculated in Appendix A. From Eq. (A.11) and (8), the approximated formula of the ASD of θ_Y is

$$\begin{aligned} \sqrt{G_{\theta_Y}(f)} &\approx \left| \frac{mh}{\kappa_Y - I_Y(2\pi f)^2} \right| \sqrt{G_{(\omega^2 \tilde{x}) * \tilde{\theta}_P}(f)} \\ &= \left| \frac{mh}{\kappa_Y - I_Y(2\pi f)^2} \right| \frac{(2\pi \times 1 \text{ Hz})^4}{g} G_{\text{seis}}(1 \text{ Hz}) \\ &\quad \times \sqrt{\frac{\pi Q f_0^5}{(f - |f_x - f_y|)^2} \left(\frac{1}{(f - 2f_0)^2} + \frac{1}{(f + 2f_0)^2} \right)}. \end{aligned} \quad (19)$$

This formula is valid at low frequencies (below ~ 0.3 Hz). Fig. 6 compares this approximation and the full calculation (Fig. 4). It shows that Eq. (19) gives a good approximation below 0.3 Hz. Several dependences on the parameters can be extracted from this formula, which are discussed below.

3.1. Vibration isolation around resonant frequencies

We have already shown that reduction of seismic vibration is effective for suppression of nonlinear noise. In particular, vibration isolation around the pendulum's resonant frequencies, which typically lie around 1 Hz for a cm – m scale pendulum, is important

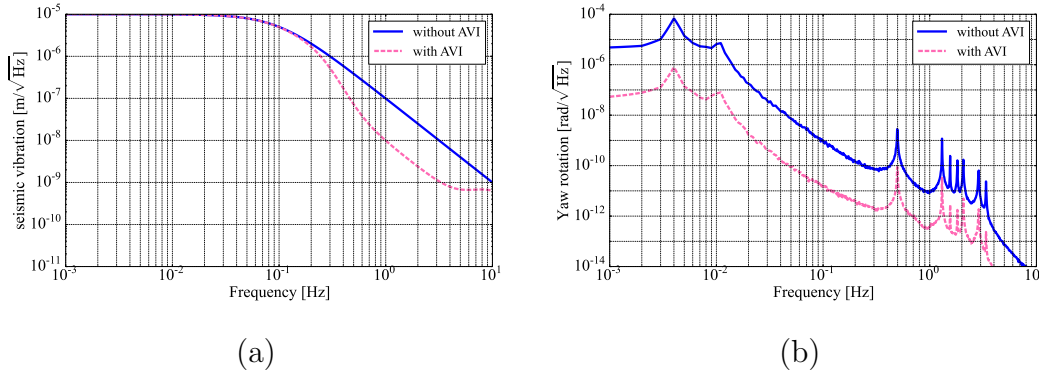


Figure 7. The amplitude spectral densities of (a) the seismic vibration and (b) nonlinear vibration noise with (dashed pink) and without (solid blue) active vibration isolation (AVI).

for broadband noise suppression. This is because the large fraction of the frequency convolution originate from the vibrations at resonant frequencies convolved with the nearby frequencies.

Several vibration isolation systems around 1 Hz or sub-Hz have been proposed. Note that when using them, we have to be careful about additional resonances, which can induce additional nonlinear noise. An active feedback system with a hexapod stage will be a good choice for this reason, because it uses a rigid system so that the additional resonant frequencies are high enough. Vibration isolation of about one order of magnitude with the hexapod system at 0.5 – 5 Hz is reported in [16].

The calculated nonlinear noise with active vibration isolation (AVI) is shown in Fig. 7. The assumed vibration is shown in Fig. 7 (a), which is the original vibration suppressed by one order of magnitude at 0.5 – 5 Hz. AVI successfully reduces nonlinear noise by two orders of magnitudes. At every frequency, it reaches almost the same noise level as the quiet case in Fig. 4, which confirms the importance of isolation around the pendulum's resonant frequencies.

3.2. Suppressing resonances

For similar reasons as the previous discussion, suppressing the resonant peaks by damping is also effective in reducing nonlinear noise. Although the Q factors of various non-torsional resonant modes do not appear explicitly in Eq. (8), the convolution terms of Eq. (8) are dependent on them. As shown in Eq. (19), nonlinear noise is proportional to \sqrt{Q} . This is because the RMS amplitude of a resonant mode is proportional to \sqrt{Q} .

Fig. 8 shows the calculated nonlinear noise with $Q = 10^3$, 10^2 and 10. All resonant peaks are assumed to have the same Q factor. As expected, lower Q gives smaller noise, and the dependence is almost proportional to \sqrt{Q} . This shows the importance of damping in terms of noise.

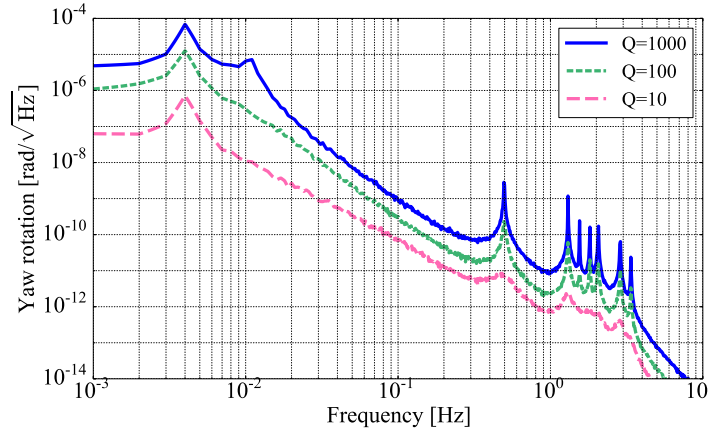


Figure 8. Q factor dependence of nonlinear vibration noise. $Q = 10^3$ (solid blue), $Q = 10^2$ (dashed green) and $Q = 10$ (long-dashed pink).

3.3. Proper choice of pendulum's parameters

Parameters of the pendulum are also important factors of nonlinear noise. Some of them appear explicitly in Eq. (8), and some are also implicitly related to \tilde{x} , \tilde{y} , $\tilde{\theta}_R$ and $\tilde{\theta}_P$ via their resonant frequencies. Additionally, they are technically related to the achievable Q factors with some damping systems. The Q factors are not in Eq. (8) explicitly, but they are related to \tilde{x} , \tilde{y} , $\tilde{\theta}_R$ and $\tilde{\theta}_P$, and approximately appears as Eq. (19). Since these issues are correlated, dependence on a parameter is a complicated question. Here we show some examples of dependence, though a complete discussion will require more consideration with a detailed set of conditions.

First we investigate the resonant frequencies. Resonant frequencies are the key factors in determining the vibration transfer function of the pendulum. As Eq. (19) shows, nonlinear noise will be proportional to $f_0^{1.5}$ at low frequencies.

Consider the case where all the resonant frequencies are scaled by the same factor while the other parameters, such as h or the size of the suspended bar, are fixed. Though this assumption is a little unrealistic because resonant frequencies are determined by the parameters, we want to extract only the dependence on the resonant frequencies here. In this case, nonlinear noise will change as in Fig. 9. The dependence on the resonant frequencies is roughly as expected at low frequencies. Therefore we should set resonant frequencies lower.

Note that this simple dependence is true only when the seismic vibration spectrum is a simple function of frequency. The actual spectrum has some structure as shown in Fig. 3, so there may be an optimal choice of resonant frequencies.

Suppression of the Q factor gives an additional reduction of nonlinear noise in proportion to \sqrt{Q} (long-dashed orange line in Fig. 9). The same dependence on the Q factor as shown in Fig. 8 is true even if the resonant frequencies are different.

Next we discuss the size of the pendulum. When every length (l , h , and size) scales

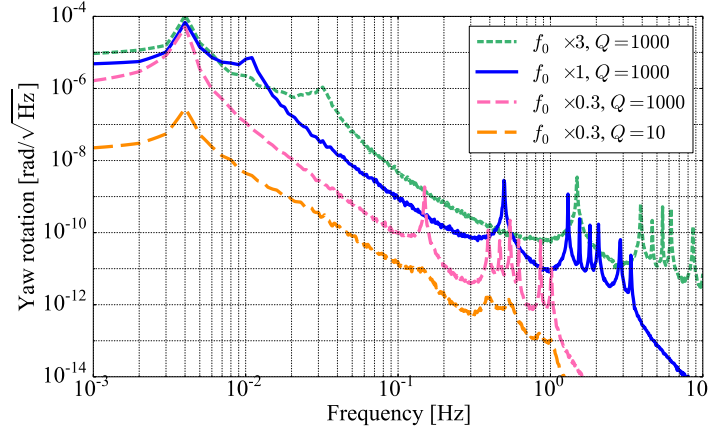


Figure 9. Dependence on resonant frequencies. All the resonant frequencies are scaled by $\times 3$ (dashed green), $\times 1$ (solid blue) and $\times 1/3$ (long-dashed pink) in case of $Q = 1000$. Additionally, the longer-dashed orange line shows the nonlinear noise when the resonant frequencies are scaled by $\times 1/3$ and the Q factor is suppressed to 10.

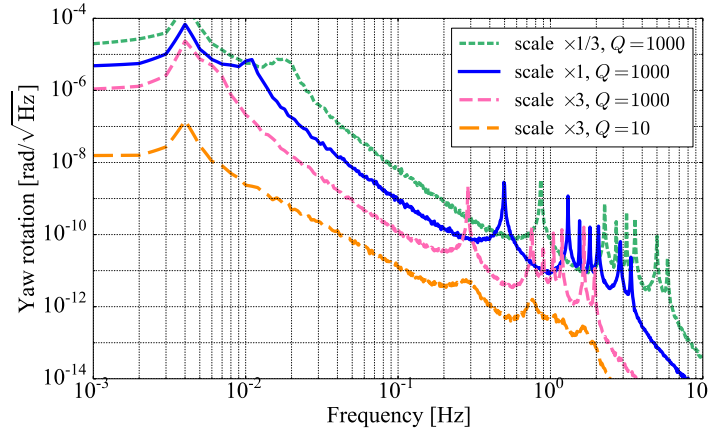


Figure 10. Nonlinear noise when the pendulum scales by $1/3$ (dashed green), 1 (solid blue) and 3 (long-dashed pink). The longer-dashed orange line shows the nonlinear noise when the pendulum scales by $\times 3$ and the Q factor is suppressed to 10.

by the same factor, $1/3$, 1 or 3 , nonlinear noise will change as seen in Fig. 10. It shows a rough proportionality to the inverse-square of the scaling factor. This is partly because the dominant term of Eq. (8) is proportional to mh/I_Y , which in turn is proportional to the inverse of the scaling factor. The change of resonant frequencies, which was discussed above, also contributes. The resonant frequencies are given by Eq. (18), so all of them are proportional to the inverse square-root of the scaling factor. The total dependence of noise can be explained by these two factors.

Additional reduction can be achieved by reducing the Q factor in conjunction as shown in Fig. 10 (long-dashed orange line).

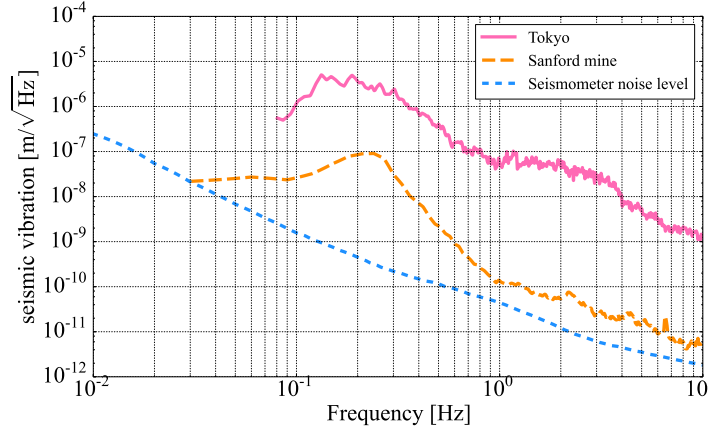


Figure 11. The ASD of seismic vibration at Sanford mine in the U.S. (dashed orange) [15] and the instrumental self-noise level of a low-noise seismometer (dotted blue) [17], which gives the achievable vibration level with an active vibration isolation.

4. Discussion

Taking into account nonlinear vibration transfer in the mechanical system, sensitivity of a 30 cm scale pendulum is limited to 10^{-9} rad/ $\sqrt{\text{Hz}}$ at 0.1 Hz (Fig. 4) in a noisy environment like Tokyo without any active vibration isolation ($\sim 10^{-7}$ m/ $\sqrt{\text{Hz}}$ at 1 Hz (Fig. 3)) or passive damping of the other pendulum modes ($Q = 1000$). In terms of torque, this corresponds to 3×10^{-11} N·m/ $\sqrt{\text{Hz}}$. These values are much larger than the target sensitivity for the usage of gravity gradient measurement, which is 10^{-15} rad/ $\sqrt{\text{Hz}}$ at 0.1 Hz for EEW, and 10^{-19} rad/ $\sqrt{\text{Hz}}$ at 0.1 Hz for GW observation. Hence we need a strategy to suppress nonlinear noise by at least six orders of magnitude at 0.1 Hz.

As shown in Fig. 7 (b), vibration isolation around the resonant frequency by one order of magnitude reduces nonlinear noise by two orders of magnitude. Hence if the vibration of the top suspension point is suppressed by two more orders of magnitudes, to 10^{-10} m/ $\sqrt{\text{Hz}}$ around 1 Hz, nonlinear noise of a 30 cm scale pendulum will be reduced by four more orders of magnitude and reach 10^{-15} rad/ $\sqrt{\text{Hz}}$ at 0.1 Hz. Fig. 11 shows the ASD of the noise level of low-noise seismometers [17], which is below 10^{-10} m/ $\sqrt{\text{Hz}}$ around 1 Hz. Hence an active vibration isolation system with seismometers can suppress the vibration down to this noise level in principle. By using such a system, nonlinear noise for the 30 cm scale pendulum is reduced to below 10^{-15} rad/ $\sqrt{\text{Hz}}$ at 0.1 Hz as shown in Fig. 12, which satisfies the requirement for EEW. Note that careful design is required to realize the active vibration isolation system. In particular, tilt-horizontal coupling can be a problem [18], so some form of tiltmeter for the decoupling may be necessary. Even if it is technically difficult, additional noise reduction by damping or tuning of the resonant frequency can ease the requirement. For example, when the resonances are damped to $Q = 10$, the vibration of the top suspension point can be $\sqrt{10} \sim 3$ times larger than the value above (Fig. 8).

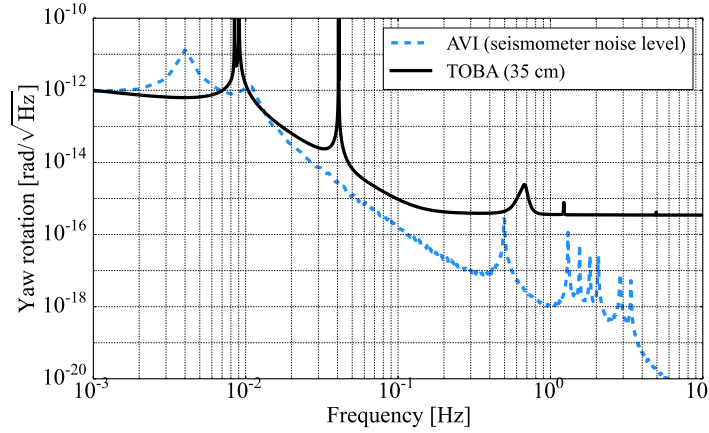


Figure 12. The achievable nonlinear noise level for the 30 cm scale pendulum by actively suppressing the vibration to the noise level of the low-noise seismometer (dotted blue). The Q factors are set to 1000.

If we choose a seismically quiet site to build the detector, nonlinear noise can be reduced more easily. It is reported that the vibration at Sanford mine in the U.S. is $10^{-10} \text{ m}/\sqrt{\text{Hz}}$ at 1 Hz [15]. The ASD is shown in Fig. 11 with the seismic vibration in Tokyo and the noise level of low-noise seismometers. However, note that we may not always have an arbitrary choice of site for the purpose of earthquake early warning. Though optimal arrangement of sensors is under investigation, some of the detectors will be placed near the city the system is meant to protect, where vibration tends to be large. Therefore, designing an isolation system is necessary.

For gravitational wave observations, 10 m scale pendulums are planned [6]. The parameters are listed in Table 2. Since the design of the wire length and the suspension point height is not fixed yet, arbitral values of $l = 2 \text{ m}$ and $h = 0.15 \text{ m}$ are set for them here. By applying the scale dependence which was discussed above in Fig. 10, we can expect three orders of magnitude noise suppression compared with 30 cm. Additionally, the active vibration isolation using the low-noise seismometers can suppress the vibration by 3.5 orders of magnitude in Tokyo (Fig. 11), which will reduce nonlinear noise by seven orders of magnitude more. Damping to $Q = 10$ gives an additional reduction of one order of magnitude. In total, eleven orders of magnitude reduction can be expected, which results in nonlinear noise of $10^{-20} \text{ rad}/\sqrt{\text{Hz}}$ at 0.1 Hz. Though we can choose seismically quiet sites such as Sanford mine to build in for the lower level of seismic vibration, the advantage of Sanford mine is not significant since the resonant frequencies are lower than the 30 cm scale pendulum as listed in Table 2. The difference of the vibration ASD between Tokyo and Sanford mine is only 1.5 orders of magnitude at the resonant frequencies (sub-Hz) (Fig. 11), so only three orders of magnitude suppression is expected for nonlinear noise. Therefore active vibration isolation is essential again for this case. Fig. 13 shows nonlinear noise of a 10 m scale pendulum if it is placed at Sanford mine or

Table 2. The parameters of 10 m scale TOBA.

parameter		symbol	value	unit
mass		m	7600	kg
moment of inertia	(Pitch)	I_P	6.4×10^4	$\text{kg}\cdot\text{m}^2$
	(Roll)	I_R	3.4×10^2	$\text{kg}\cdot\text{m}^2$
	(Yaw)	I_Y	6.4×10^4	$\text{kg}\cdot\text{m}^2$
length of wire		l	2	m
suspension point height		h	0.15	m
Q factors		Q_x, Q_y, Q_P, Q_R	10	-
resonant frequency	translation (x)	f_x	0.353	Hz
	translation (y)	f_y	0.337	Hz
	Pitch	f_P	0.952	Hz
	Roll	f_R	0.066	Hz

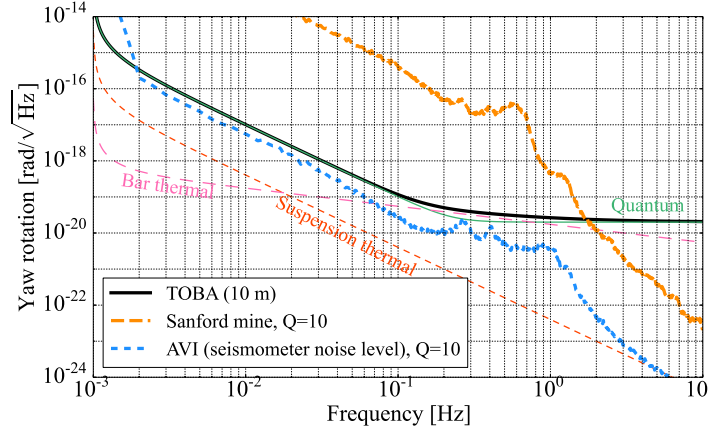


Figure 13. The achievable nonlinear noise level for the 10 m scale pendulum by placing the detector at Sanford mine (dashed orange) or actively suppressing the vibration to the noise level of the low-noise seismometer (dotted blue), plotted with other noise sources (solid green : quantum noise, dashed red : suspension thermal noise, long-dashed pink : bar thermal noise [6]). The Q factors are set to 10.

the vibration is actively suppressed to the noise level of a seismometer. $10^{-19} \text{ rad}/\sqrt{\text{Hz}}$ at 0.1 Hz, the level of quantum noise and thermal noise of the bar, is shown to be achievable by combining the active vibration isolation system with damping.

These rough plans give us a prospect to reach the target sensitivities as a gravity gradiometer. For more strict calculations, however, detailed design of the suspension system and the structure of seismic vibration spectrum have to be taken into account. Though we do not go into the details of this here, it will be necessary when doing case studies.

5. Conclusion

We have discussed about how the rotational noise of a torsion pendulum is introduced nonlinearly from seismic vibrations. The ASD of the noise can reach 10^{-9} rad/ $\sqrt{\text{Hz}}$ at 0.1 Hz for a 30 cm scale pendulum in locations with noisy seismic vibrations such as Tokyo. Based on the investigation in Sec. 3, we have created a rough strategy to reduce the noise down to the target sensitivity, 10^{-15} rad/ $\sqrt{\text{Hz}}$ at 0.1 Hz for EEW and 10^{-19} rad/ $\sqrt{\text{Hz}}$ for GW at 0.1 Hz. They are achievable in principle by combining the following; active vibration isolation, damping system, increasing the size of the pendulum or going to seismically quiet site. Note that a strict estimation of noise will require a case study based on the detailed design of the suspension system and the actual seismic vibration spectrum.

Acknowledgments

The work about TOBA is supported by JSPS KAKENHI Grants Number JP16H03972, JP24244031 and JP18684005. We thank Ooi Ching Pin for editing this paper.

Appendix A. Convolution of the translation \tilde{x} and the rotation $\tilde{\theta}_P$

The frequency convolution $(\omega^2 \tilde{x}) * \tilde{\theta}_P$ is calculated in this appendix.

First, based on Eq. (14) and (16), the Fourier spectrum of \tilde{x} and $\tilde{\theta}_P$ can be approximated as follows around the translational resonant frequency f_x or f_y , with

$$\tilde{x}(f) \simeq \frac{f_x^2}{f_x^2 + i\frac{f_x}{Q_x}f - f^2} \left(\frac{1\text{Hz}}{f}\right)^2 \tilde{x}_g(1\text{Hz}) \quad (\text{A.1})$$

and

$$\tilde{\theta}_P(f) \simeq \frac{4\pi^2 f_y^2 f^2}{g(f_y^2 + i\frac{f_y}{Q_y}f - f^2)} \left(\frac{1\text{Hz}}{f}\right)^2 \tilde{y}_g(1\text{Hz}). \quad (\text{A.2})$$

Here the seismic vibration is assumed to be proportional to inverse-square of frequency. $\tilde{x}_g(1\text{Hz})$ and $\tilde{y}_g(1\text{Hz})$ are the Fourier spectrum of the seismic vibration at 1 Hz. These are converted from the amplitude spectral density of the seismic vibration $\sqrt{G_{\text{seis}}(f)}$ as

$$\tilde{x}_g(f) = \sqrt{\frac{T}{8\pi^2}} \sqrt{G_{\text{seis}}(f)} e^{i\theta_x(f)} \quad (\text{A.3})$$

and

$$\tilde{y}_g(f) = \sqrt{\frac{T}{8\pi^2}} \sqrt{G_{\text{seis}}(f)} e^{i\theta_y(f)}. \quad (\text{A.4})$$

T is the time length used for the calculation. The dependence on T disappears later when the results are re-converted to ASD. Here the phase of the Fourier spectrums,

$\theta_x(f)$ and $\theta_y(f)$, are assumed to be random at each frequency and independent between x and y . Then the convolution around the translational resonant frequency $f_x \simeq f_y$ is

$$\begin{aligned} & (\omega^2 \tilde{x}) * \tilde{\theta}_P(f) \\ &= \frac{(2\pi)^4 (1 \text{ Hz})^4}{g} \frac{T}{8\pi^2} G_{\text{seis}}(1 \text{ Hz}) \\ & \quad \times \int_{f_0-\Delta f}^{f_0+\Delta f} \frac{f_x^2}{f_x^2 + i\frac{f_x}{Q_x}(f-\alpha) - (f-\alpha)^2} \frac{f_y^2}{f_y^2 + i\frac{f_y}{Q_y}\alpha - \alpha^2} e^{i(\theta_x(f-\alpha) + \theta_y(\alpha))} d\alpha. \end{aligned} \quad (\text{A.5})$$

Here $f_0 = (f_x + f_y)/2 \simeq f_x \simeq f_y$, and Δf is the frequency range of convolution, which is chosen to cover the resonant peaks of x and θ_P ($f_0 = 0.9 \text{ Hz}$ and $\Delta f = 0.2 \text{ Hz}$ in Fig. 5). The frequency f is limited to within $|f| < \Delta f$. Since the integrand has large value only around f_0 , the integral range can be extended to $[0, \infty]$ in approximation. Then the integral part can be modified to

$$(\text{integral}) \approx \int_0^\infty A_f(\alpha) e^{i\theta(\alpha)} e^{i\alpha t} d\alpha \quad (\text{A.6})$$

where

$$A_f(\alpha) \equiv \frac{f_x^2}{f_x^2 + i\frac{f_x}{Q_x}(f-\alpha) - (f-\alpha)^2} \frac{f_y^2}{f_y^2 + i\frac{f_y}{Q_y}\alpha - \alpha^2} \quad (\text{A.7})$$

and

$$\theta(\alpha) = \theta_x(f-\alpha) + \theta_y(\alpha) - \alpha t. \quad (\text{A.8})$$

Due to the randomness of θ_x and θ_y , $\theta(\alpha)$ is a random phase independent to t , so Eq. (A.6) is a Fourier transform of $A_f(\alpha) e^{i\theta(\alpha)}$. Therefore, the mean power of $(\omega^2 \tilde{x}) * \tilde{\theta}_P(f)$ is

$$\begin{aligned} \left\langle |(\omega^2 \tilde{x}) * \tilde{\theta}_P(f)|^2 \right\rangle &= \left(\frac{(2\pi \times 1 \text{ Hz})^4}{g} \frac{T}{8\pi^2} G_{\text{seis}}(1 \text{ Hz}) \right)^2 \left\langle |\mathcal{F} \cdot \mathcal{T} \cdot [A_f(\alpha) e^{i\theta(\alpha)}]|^2 \right\rangle \\ &= \left(\frac{(2\pi \times 1 \text{ Hz})^4}{g} \frac{T}{8\pi^2} G_{\text{seis}}(1 \text{ Hz}) \right)^2 \int_0^\infty G_A(\alpha) d\alpha. \end{aligned} \quad (\text{A.9})$$

G_A is the power spectral density of $A_f(\alpha) e^{i\theta(\alpha)}$, so

$$\begin{aligned} \int_0^\infty G_A(\alpha) d\alpha &= \int_0^\infty \frac{8\pi^2}{T} |A_f(\alpha) e^{i\theta(\alpha)}|^2 \\ &= \frac{8\pi^2}{T} \int_0^\infty \frac{f_x^4 f_y^4}{|f_x^2 + i\frac{f_x}{Q_x}(f-\alpha) - (f-\alpha)^2|^2 |f_y^2 + i\frac{f_y}{Q_y}\alpha - \alpha^2|^2} d\alpha \\ &\approx \frac{8\pi^2}{T} \frac{\pi Q f_0^5}{(f - |f_x - f_y|)^2} \left(\frac{1}{(f - 2f_0)^2} + \frac{1}{(f + 2f_0)^2} \right). \end{aligned} \quad (\text{A.10})$$

Here $Q_x = Q_y \equiv Q \gg 1$ and $|f_x - f_y| \ll f_0$ is assumed for simplicity. From Eq. (A.9) and (A.10), the amplitude spectral density of the convolution $(\omega^2 \tilde{x}) * \tilde{\theta}_P(f)$ is

$$\begin{aligned} \sqrt{G_{(\omega^2 \tilde{x}) * \tilde{\theta}_P}(f)} &= \sqrt{\frac{8\pi^2}{T} \left\langle |(\omega^2 \tilde{x}) * \tilde{\theta}_P(f)|^2 \right\rangle} \\ &= \frac{(2\pi \times 1 \text{ Hz})^4}{g} G_{\text{seis}}(1 \text{ Hz}) \sqrt{\frac{\pi Q f_0^5}{(f - |f_x - f_y|)^2} \left(\frac{1}{(f - 2f_0)^2} + \frac{1}{(f + 2f_0)^2} \right)}. \end{aligned} \quad (\text{A.11})$$

This gives an approximation of nonlinear noise which is valid at low frequencies (below ~ 0.2 Hz) as discussed in Sec. 3.

References

- [1] C. D. Hoyle, D. J. Kapner, B. R. Heckel, E. G. Adelberger, J. H. Gundlach, U. Schmidt, and H. E. Swanson. Submillimeter tests of the gravitational inverse-square law. *Phys. Rev. D*, 70:042004, Aug 2004.
- [2] Wen-Hai Tan, Shan-Qing Yang, Cheng-Gang Shao, Jia Li, An-Bin Du, Bi-Fu Zhan, Qing-Lan Wang, Peng-Shun Luo, Liang-Cheng Tu, and Jun Luo. New test of the gravitational inverse-square law at the submillimeter range with dual modulation and compensation. *Phys. Rev. Lett.*, 116:131101, Mar 2016.
- [3] T. J. Quinn, C. C. Speake, S. J. Richman, R. S. Davis, and A. Picard. A new determination of G using two methods. *Phys. Rev. Lett.*, 87:111101, Aug 2001.
- [4] Liang-Cheng Tu, Qing Li, Qing-Lan Wang, Cheng-Gang Shao, Shan-Qing Yang, Lin-Xia Liu, Qi Liu, and Jun Luo. New determination of the gravitational constant g with time-of-swing method. *Phys. Rev. D*, 82:022001, Jul 2010.
- [5] Riley Newman, Michael Bantel, Eric Berg, and William Cross. A measurement of g with a cryogenic torsion pendulum. *Philosophical Transactions of the Royal Society of London A: Mathematical, Physical and Engineering Sciences*, 372(2026), 2014.
- [6] Masaki Ando, Koji Ishidoshiro, Kazuhiro Yamamoto, Kent Yagi, Wataru Kokuyama, Kimio Tsubono, and Akiteru Takamori. Torsion-bar antenna for low-frequency gravitational-wave observations. *Phys. Rev. Lett.*, 105:161101, Oct 2010.
- [7] Koji Ishidoshiro, Masaki Ando, Akiteru Takamori, Hirotaka Takahashi, Kenshi Okada, Nobuyuki Matsumoto, Wataru Kokuyama, Nobuyuki Kanda, Yoichi Aso, and Kimio Tsubono. Upper limit on gravitational wave backgrounds at 0.2 hz with a torsion-bar antenna. *Phys. Rev. Lett.*, 106:161101, Apr 2011.
- [8] Ayaka Shoda, Yuya Kuwahara, Masaki Ando, Kazunari Eda, Kodai Tejima, Yoichi Aso, and Yousuke Itoh. Ground-based low-frequency gravitational-wave detector with multiple outputs. *Phys. Rev. D*, 95:082004, Apr 2017.
- [9] J. Harms, J.-P. Ampuero, M. Barsuglia, E. Chassande-Mottin, J.-P. Montagner, S. N. Somala, and B. F. Whiting. Transient gravity perturbations induced by earthquake rupture. *Geophysical Journal International*, 201(3):1416–1425, 2015.
- [10] Jean-Paul Montagner, Kévin Juhel, Matteo Barsuglia, Jean Paul Ampuero, Eric Chassande-Mottin, Jan Harms, Bernard Whiting, Pascal Bernard, Eric Clévéde, and Philippe Lognonné. Prompt gravity signal induced by the 2011 tohoku-oki earthquake. *Nature Communications*, 7:13349 EP –, 11 2016.
- [11] Martin Vallée, Jean Paul Ampuero, Kévin Juhel, Pascal Bernard, Jean-Paul Montagner, and Matteo Barsuglia. Observations and modeling of the elastogravity signals preceding direct seismic waves. *Science*, 358(6367):1164–1168, 2017.
- [12] D J McManus, P W F Forsyth, M J Yap, R L Ward, D A Shaddock, D E McClelland, and B J J Slagmolen. Mechanical characterisation of the torpedo: a low frequency gravitational force sensor. *Classical and Quantum Gravity*, 34(13):135002, 2017.
- [13] D. J. McManus, P. W. F. Forsyth, N. A. Holland, R. L. Ward, D. A. Shaddock, D. E. McClelland, and B. J. J. Slagmolen. Early Earthquake Detection with a Dual Torsion-Beam Gravimeter. *arXiv*, 1809.04787, 2018.
- [14] Tomofumi Shimoda, Naoki Aritomi, Ayaka Shoda, Yuta Michimura, and Masaki Ando. Seismic cross-coupling noise in torsion pendulums. *Phys. Rev. D*, 97:104003, May 2018.
- [15] Rana X. Adhikari. Gravitational radiation detection with laser interferometry. *Rev. Mod. Phys.*, 86:121–151, Feb 2014.

- [16] Takafumi Ushiba. Laser frequency stabilization with a cryogenic optical cavity. *Ph.D thesis* (http://t-munu.phys.s.u-tokyo.ac.jp/theses/ushiba_thesis.pdf), 2015.
- [17] C. Collette and F. Matichard. Sensor fusion methods for high performance active vibration isolation systems. *Journal of Sound and Vibration*, 342:1 – 21, 2015.
- [18] Krishna Venkateswara, Charles A. Hagedorn, Matthew D. Turner, Trevor Arp, and Jens H. Gundlach. A high-precision mechanical absolute-rotation sensor. *Review of Scientific Instruments*, 85(1):015005, 2014.